

Intraseasonal Sea Surface Temperature Variability across the Indonesian Seas

The Faculty of Oregon State University has made this article openly available.
Please share how this access benefits you. Your story matters.

Citation	Napitu, A. M., Gordon, A. L., & Pujiana, K. (2015). Intraseasonal Sea Surface Temperature Variability across the Indonesian Seas. <i>Journal of Climate</i> , 28(22), 8710-8727. doi:10.1175/JCLI-D-14-00758.1
DOI	10.1175/JCLI-D-14-00758.1
Publisher	American Meteorological Society
Version	Version of Record
Terms of Use	http://cdss.library.oregonstate.edu/sa-termsfuse

Intraseasonal Sea Surface Temperature Variability across the Indonesian Seas*

ASMI M. NAPITU⁺ AND ARNOLD L. GORDON

Lamont-Doherty Earth Observatory, Columbia University, Palisades, New York

KANDAGA PUJIANA[#]

College of Earth, Ocean, and Atmospheric Sciences, Oregon State University, Corvallis, Oregon

(Manuscript received 6 November 2014, in final form 15 August 2015)

ABSTRACT

Sea surface temperature (SST) variability at intraseasonal time scales across the Indonesian Seas during January 1998–mid-2012 is examined. The intraseasonal variability is most energetic in the Banda and Timor Seas, with a standard deviation of 0.4°–0.5°C, representing 55%–60% of total nonseasonal SST variance. A slab ocean model demonstrates that intraseasonal air–sea heat flux variability, largely attributed to the Madden–Julian oscillation (MJO), accounts for 69%–78% intraseasonal SST variability in the Banda and Timor Seas. While the slab ocean model accurately reproduces the observed intraseasonal SST variations during the northern winter months, it underestimates the summer variability. The authors posit that this is a consequence of a more vigorous cooling effect induced by ocean processes during the summer. Two strong MJO cycles occurred in late 2007–early 2008, and their imprints were clearly evident in the SST of the Banda and Timor Seas. The passive phase of the MJO [enhanced outgoing longwave radiation (OLR) and weak zonal wind stress] projects on SST as a warming period, while the active phase (suppressed OLR and westerly wind bursts) projects on SST as a cooling phase. SST also displays significant intraseasonal variations in the Sulawesi Sea, but these differ in characteristics from those of the Banda and Timor Seas and are attributed to ocean eddies and atmospheric processes independent from the MJO.

1. Introduction

Various processes, both local and remote, govern sea surface temperature (SST) variability across the Indonesian Seas, often referred to as the Maritime Continent. Local processes include intense tidal mixing, Ekman dynamics, and air–sea heat fluxes (Gordon 2005; Sprintall et al. 2014). The Indonesian Seas SST is also sensitive to the large-scale climate of the Indo-Pacific region, such as El Niño–Southern Oscillation (ENSO), the Indian Ocean dipole (IOD) (McBride et al. 2003),

and the seasonal forcing of the Asian–Australian monsoon, which is the largest contributor to SST variability within the Indonesian Seas (Qu et al. 2005; Kida and Richards 2009; Halkides et al. 2011). Furthermore, the Maritime Continent falls along the pathway of the Madden–Julian oscillation (MJO), an intraseasonal tropical atmospheric phenomenon consisting of convective and subsidence cells propagating eastward from the Indian Ocean to the Pacific Ocean affecting weather across the tropics and midlatitude (Waliser et al. 1999; Madden and Julian 1994; Zhang 2005).

The Indonesian Seas are characterized by warmer SST over their Southern Hemisphere region during the boreal winter months of December–February (DJF). The months of DJF are also marked with increased precipitation over the Indonesian Maritime Continent (Tanaka 1994). Colder SST characterizes the Indonesian Seas during the boreal summer months of June–August (JJA), during which time the climate is somewhat drier, particularly its Southern Hemisphere region, as the intertropical convergence zone shifts to the north of the equator (Meehl 1987).

* Lamont-Doherty Earth Observatory Contribution Number 7926.

⁺ Additional affiliation: Ministry of Marine Affairs and Fisheries of the Republic of Indonesia.

[#] Additional affiliation: Faculty of Earth Sciences and Technology, Institut Teknologi Bandung, Bandung, Indonesia.

Corresponding author address: Asmi Napitu, Lamont-Doherty Earth Observatory, 61 Route 9W, Palisades, NY 10964.
E-mail: asmi@ldeo.columbia.edu

By applying an empirical orthogonal function (EOF) to a ~ 15 -yr SST dataset (see [section 2](#)), extending from January 1998 to mid-2012, we find that seasonal variability explains about 52% of SST variability over the Indonesian Seas. At shorter time scales, variability at semiannual time scales accounts for about 18% of SST in the Indonesian Seas. This semiannual component occurs during the monsoon transition period, during which solar insolation is increased and wind is weaker, which results in warmer SST ([Halkides et al. 2011](#)).

The combined seasonal and semiannual variability can explain about 70% of total SST variances in the Indonesian Seas. The remaining 30% of the SST variability is attributed to intraseasonal and interannual variations. As for intraseasonal SST variability, previous studies suggested that SST perturbation with periods less than 120 days over the Indo-Pacific region is dictated by the MJO ([Duvel and Vialard 2007](#); [Drushka et al. 2012](#)). [Drushka et al. \(2012\)](#) argued that surface heat flux attributed to the MJO dominates mixed layer heat budget variability in the region. The MJO activity over the western Pacific warm pool is suggested to be linked and interact with ENSO. [Waliser et al. \(1999\)](#) and [Kessler \(2001\)](#) showed that MJO signature increases over the warm pool during the development of the ENSO warm phase, and the increased MJO activity shifts farther east as El Niño is fully developed.

The MJO–ocean interaction is likely not confined to atmospheric impact on a passive ocean as MJO-induced intraseasonal SST variability potentially feeds back to the atmosphere through modifying the surface flux, which in turn affects the MJO evolution if the subsurface cooler waters enter the surface layer ([Shinoda et al. 1998](#)). The most active period for MJO activity, indicated by a strong signature of eastward propagation from the Indian Ocean to the Pacific Ocean, takes place between late fall and early spring, during which the warm pool has its greatest east–west extent ([Salby and Hendon 1994](#)).

Given the MJO influence on ENSO and the potential feedback that intraseasonal SST may provide to the atmosphere over the Maritime Continent, with potential impact on MJO behavior en route from the tropical Indian Ocean to the western Pacific Ocean warm pool, we examine intraseasonal SST variability of the Indonesian Seas, specifically the SST response to strong MJO events, which we argue is one of the primary drivers for SST variability at intraseasonal time scales in large expanses of the Indonesian Seas. Other factors that might influence intraseasonal SST variability include eddies and planetary waves ([Qiu et al. 1999](#); [Wijffels and Meyers 2004](#)). [Drushka et al. \(2010\)](#) suggested that the intraseasonal Kelvin waves originating in the equatorial Indian Ocean propagate along the southern coasts of the Indonesian archipelago. These

waves manage to squeeze through several narrow straits into the internal Indonesian Seas and affect the thermocline and SST variability along their paths ([Pujiana et al. 2013](#)). Intraseasonal eddies are also abundant in the Indonesian Seas and might perturb SST ([Qiu et al. 1999](#)).

This study, which focuses on the Indonesian region of the Maritime Continent, complements similar studies investigating intraseasonal SST variability in the neighboring and broader Indo-Pacific region ([Duvel et al. 2004](#); [Vialard et al. 2013](#)). We begin with describing the data and method in [section 2](#). [Section 3](#) presents general characteristics and generation mechanisms of intraseasonal SST in the Indonesian Seas. This section aims to elucidate key intraseasonal SST features and their genesis, which include the role of MJO surface heat flux in governing intraseasonal SST variability in the Indonesian Seas. The intraseasonal SST responses to strong MJO events across the Indonesian Seas are presented in [section 4](#). We conclude the paper with a summary and discussion in [section 5](#).

2. Data and methods

a. Datasets

The main data used in this study are the SST data from the Tropical Rainfall Measuring Mission (TRMM) Microwave Imager (TMI) satellite acquired during January 1998–June 2012. The gridded satellite-derived SST data have a spatial resolution of $0.25^\circ \times 0.25^\circ$ and a sampling interval Δt of 7 days, and the region of interest is within longitudes of 90° – 140° E and latitudes of 10° N– 15° S. Previous studies (e.g., [Kida and Richards 2009](#)) found that the TMI data are better than radiometric satellite data because the TMI data contain fewer gaps as a result of the ability of the TMI satellite to penetrate cloud cover ([Wentz et al. 2000](#)). In addition to SST, we also analyze the precipitation data from the TMI product.

The outgoing longwave radiation (OLR) is examined to relate intraseasonal variability within the atmosphere to SST variability, as the OLR is commonly used as a good indicator to study convective activity. The OLR data have a spatial resolution of $2.5^\circ \times 2.5^\circ$ and are sampled daily ([Liebmann and Smith 1996](#)). The data used for this study extend from January 1998 to June 2012. Wind data, from the level-3.5A gridded cross-calibrated multiple platform (CCMP) product, 1998 to 2011, have a spatial resolution of $0.25^\circ \times 0.25^\circ$ ([Ardizzone et al. 2009](#)). The OLR, precipitation, and wind data encompass the same region as that of the SST data.

For surface heat flux analyses, we utilize reanalysis TropFlux products ([Praveen Kumar et al. 2012](#))

consisting of shortwave, latent, longwave, and sensible heat fluxes from 1978 to mid-2012 with daily time resolution and a spatial resolution of $1^\circ \times 1^\circ$, showing a good agreement with the surface heat flux data observed from equatorial moorings in the Indian and Pacific Oceans. We find that the TropFlux reanalysis data are useful for our analysis because they consistently exhibit intraseasonal features over the Indonesian Maritime Continent, which reasonably agrees with those from satellite-derived data.

The mixed layer depth information is important to estimate the influence of surface heat flux on SST. In our study, we use the mixed layer depth data from a climatological dataset with a spatial resolution of $2^\circ \times 2^\circ$ from [de Boyer Montégut et al. \(2004\)](#).

In addition to the above main datasets, we analyze the gridded sea level anomaly (SLA) product from Archiving, Validation, and Interpretation of Satellite Oceanographic Data (AVISO) ([Ducet et al. 2000](#)). The satellite-derived SLA has a horizontal resolution of $0.25^\circ \times 0.25^\circ$ and temporal resolution of 7 days.

b. Methods

To extract the main characteristics of intraseasonal variability from the data, we employ statistical methods and a slab ocean model. The details of the statistical methods and the model are explained below.

1) STATISTICAL METHODS

- The monthly climatological mean is removed.
- The intraseasonal variability is obtained through applying a bandpass filter with cutoff periods of 21 days and 119 days, resulting in the filtered data with oscillations varying between 21 and 119 days.
- Dominant periods characterizing intraseasonal variability of the data are identified by applying spectral analyses. The confidence interval for the spectrum estimate $P(f)$ is defined as $[(\nu - 1)s^2(f)/\chi_{1-\alpha/2,\nu}^2] < P(f) < [(\nu - 1)s^2(f)/\chi_{\alpha/2,\nu}^2]$, where ν denotes the degrees of freedom, $s^2(f)$ is the observed standard deviation, χ^2 is the cumulative chi-square distribution value, and α is the level of significance.
- The degree of correlation in frequency domain between two time series is examined using a coherence or cross-wavelet transform method. The confidence level for the squared coherence $\gamma_{(1-\alpha)}^2$ is given as $\gamma_{(1-\alpha)}^2 = 1 - \alpha^{2/(\nu-2)}$. The significance level of the cross-wavelet transform is approximated using a Monte Carlo method ([Grinsted et al. 2004](#)).
- The time variability of the dominant oscillations is investigated using a wavelet method. The confidence level of the wavelet transform $W_n(s)$ is defined as

$W_n(s)\chi_2^2$, where χ_2^2 is the cumulative chi-square distribution value with 2ν ([Torrence and Compo 1998](#)).

2) SLAB OCEAN MODEL

The rate of SST change is governed by heat fluxes due to air–sea interaction, ocean advection, and turbulence, which can be expressed as the following simplified surface mixed layer heat budget equation ([Wang and McPhaden 1999](#)):

$$\rho c_p h \frac{\partial T}{\partial t} = Q_o - \rho c_p h \mathbf{u} \cdot \nabla T - \frac{K_T}{h} \frac{\partial T}{\partial z} + R \quad (1)$$

where T is the average surface mixed layer temperature, Q_o the net surface heat flux, ρ the seawater density, c_p the heat capacity, h the surface mixed layer depth, \mathbf{u} the velocity, and K_T the thermal diffusivity. The terms in the right-hand side of (1) represent, from left to right, are the net surface heat flux, the ocean advective heat flux, the turbulent heat flux across the base of the surface mixed layer, and the residual flux, which accounts for horizontal divergence of eddy heat flux within the mixed layer and errors attributed to other terms in (1). The net heat flux is the sum of shortwave radiation minus the penetrative component at the base of the surface mixed layer, latent heat flux, sensible heat flux, and longwave radiation, as follows:

$$Q_o = Q_{sw}(1 - 0.45e^{-0.04h}) + Q_L + Q_S + Q_{LW}. \quad (2)$$

We can then classify the primary drivers for SST change into atmospheric and oceanic components. Since observations of heat fluxes due to ocean processes within the Indonesian Seas are not available and previous relevant studies demonstrated that surface heat fluxes contribute substantially to force surface mixed layer heat budget in the Indo-Pacific region (e.g., [Vialard et al. 2013](#)), we here consider only the atmospheric component to investigate the generation mechanisms of SST variability across the Indonesian Seas. Thus, (1) can be further simplified into

$$\rho c_p h \frac{\partial T}{\partial t} = Q_o + R, \quad (3)$$

where R now includes the advective and turbulent heat fluxes. Temporal integration of (3) results in estimated SST forced by surface heat flux. We use (3), named as a slab ocean model, to quantify the contribution of surface heat flux to control intraseasonal SST in the Indonesian Seas. We use Q_o and the monthly climatology of h from the TropFlux product ([Praveen Kumar et al. 2012](#)) and [de Boyer Montégut et al. \(2004\)](#), respectively. Since the

surface mixed layer depth data are monthly climatologies, the slab-model-derived SST does not take into account the mixed layer sub-monthly variability for our calculation. This model has been used by other similar studies in other regions (Vialard et al. 2013).

3. Intraseasonal SST variability across the Indonesian Seas

a. General characteristics

The contribution of intraseasonal variability to total SST variances is estimated from the ratio between the sum of the SST variance at intraseasonal time scales (21–119 days) to total SST variances at periods longer than 14 days, whose formula is given as

$$\text{ratio} = \frac{\int_{\omega=1/119\text{day}^{-1}}^{\omega=1/21\text{day}^{-1}} P_{\text{SST}}(\omega) d\omega}{\int_{\omega=1/7n\text{day}^{-1}}^{\omega=1/14\text{day}^{-1}} P_{\text{SST}}(\omega) d\omega}, \quad (4)$$

where n is the number of SST data at each grid point, ω is the frequency, and P_{SST} is the amplitude of the SST spectral estimate. The ratio (Fig. 1a) reveals that the largest contribution of intraseasonal SST variance to total SST variance across the deep basins of the Indonesian Seas occurs within the Banda, Timor, and Sulawesi Seas, with a ratio between 55% and 60%. Other basins, such as the Java Sea, have intraseasonal variability that explains 25%–40% of the SST variation. The average of intraseasonal SST standard deviations across the study area is generally between 0.3° and 0.5°C (Fig. 1b). The mean standard deviations in the Banda and Timor Seas vary between 0.45° and 0.5°C, while the Sulawesi Sea has a standard deviation of 0.3°C.

As mentioned above, seasonal variability accounts for 70% of SST variability. Therefore, the ratio suggests that 55%–60% of the remaining 30% can be explained by intraseasonal variability (i.e., this intraseasonal variability accounts for 16%–18% of the total SST variability). We henceforth will not discuss the characteristics of intraseasonal variability over an area with a ratio of less than 40%.

The dominant oscillations characterizing the significant intraseasonal SST across the Indonesian Seas are observed at periods of 30–70 days (Fig. 2). For the Banda and Timor Seas the intraseasonal SST signal is marked with a spectral peak of 28–42 days centered at 35 days, whose magnitude is statistically different from a background red spectrum with a confidence level of 80% (Figs. 2a,b). The Sulawesi Sea intraseasonal SST, however, is characterized by a significant spectral peak

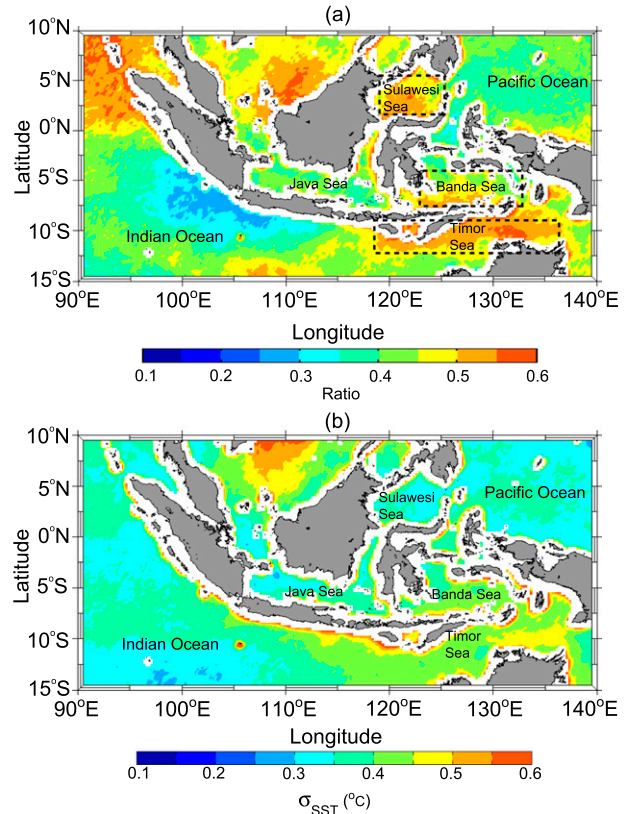


FIG. 1. (a) The significance of intraseasonal SST variability across the Indonesian Seas. The significance is inferred from the ratio between the sum of SST variances on intraseasonal time scales (21 days < period < 119 days) and the sum of SST variances with periods longer than 14 days. Dashed boxes illustrate regions with significant intraseasonal SST variability. (b) Standard deviation of intraseasonal SST across the Indonesian Seas.

centered at 56 days (Fig. 2c). In addition to the dominant 56-day period, intraseasonal SST in the Sulawesi Sea also shows another significant period of oscillation at 25 days, although with smaller spectral energy (Fig. 2c). These dominant oscillations explain more than half of the total variances attributed to intraseasonal SST in the Sulawesi Sea.

The variance of intraseasonal SST displays its strongest magnitude during the DJF period and is diminished during JJA (Fig. 3). Figure 3 shows that standard deviation of intraseasonal SST in the Banda and Timor Seas reaches up to 0.6°–0.7°C during DJF, whereas the standard deviation reduces to 0.2°–0.3°C during JJA. This agrees with Duvel and Vialard (2007), who found that intraseasonal SST across the Maritime Continent shows seasonal variability, although their standard deviation is 0.1°C smaller than our finding. The difference likely arises from the shorter extent of the time series they analyzed.

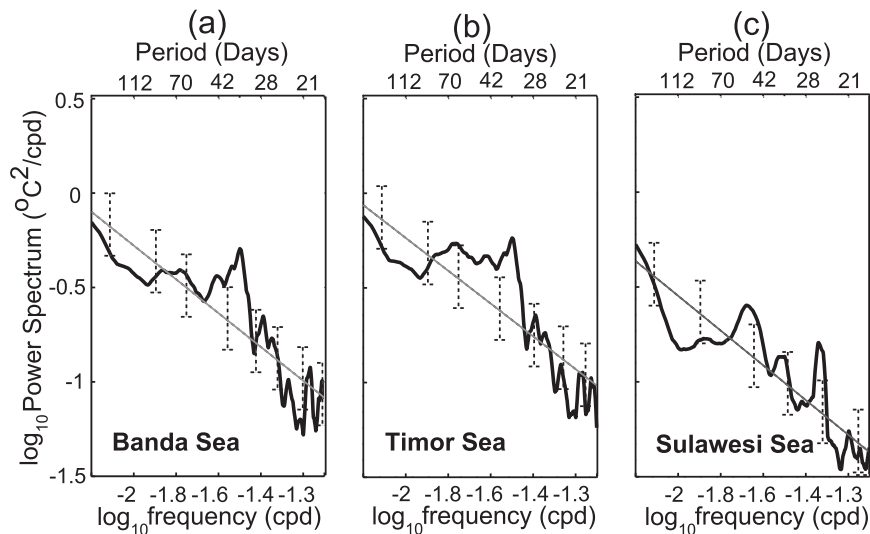


FIG. 2. Power spectrum estimates of SST (black line) in the (a) Banda Sea, (b) Timor Sea, and (c) Sulawesi Sea. Each spectrum estimate is an average over a region bounded by the dashed box shown in Fig. 1a. Gray line and error bars denote the red noise and 80% significance level, respectively.

To examine the time variability of the dominant intraseasonal SST oscillations in the Banda, Timor, and Sulawesi Seas, we apply a wavelet analysis of SST time series at each sea. The SST time series at each sea is obtained by spatially averaging SST time series for all grids within the boxes defined in Fig. 1a. A wavelet analysis of SST in the Banda and Timor Seas confirms that the magnitude of intraseasonal SST variance shows seasonal modulation, amplified during boreal winter and weak during boreal summer (Fig. 4). The analysis also suggests that the signature of amplified intraseasonal SST during boreal winter varies year by year. Unlike in the Banda and Timor Seas, the Sulawesi Sea intraseasonal SST does not reveal seasonal or interannual variability and is likely governed by processes that differ from that of the Banda and Timor Seas.

b. Generation mechanism

1) BANDA AND TIMOR SEAS

We have demonstrated that SSTs in the Banda and Timor Seas at intraseasonal time scales shows similar characteristics in their spectral peaks and seasonal patterns (Figs. 2 and 3). A coherence analysis between the basin-averaged SST time series in the Banda Sea and that in the Timor Sea shows that their intraseasonal variations are strongly coherent with $r^2 = 0.85$. Moreover, the coherent intraseasonal SSTs in the Banda and Timor Seas are also in phase, indicative of a shared forcing mechanism for the intraseasonal SST variability. Duvel and Vialard (2007) suggested that

the mechanism that controls intraseasonal variation over the Indo-Pacific region is related to eastward-propagating tropical convection originating from the Indian Ocean. We suspect that surface heat flux

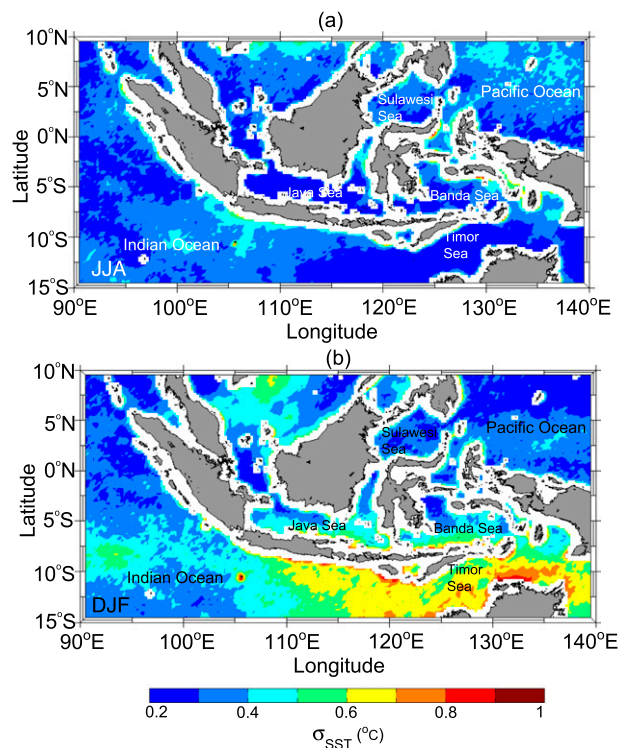


FIG. 3. Standard deviation of intraseasonal SST across the Indonesian Seas averaged over (a) JJA and (b) DJF.

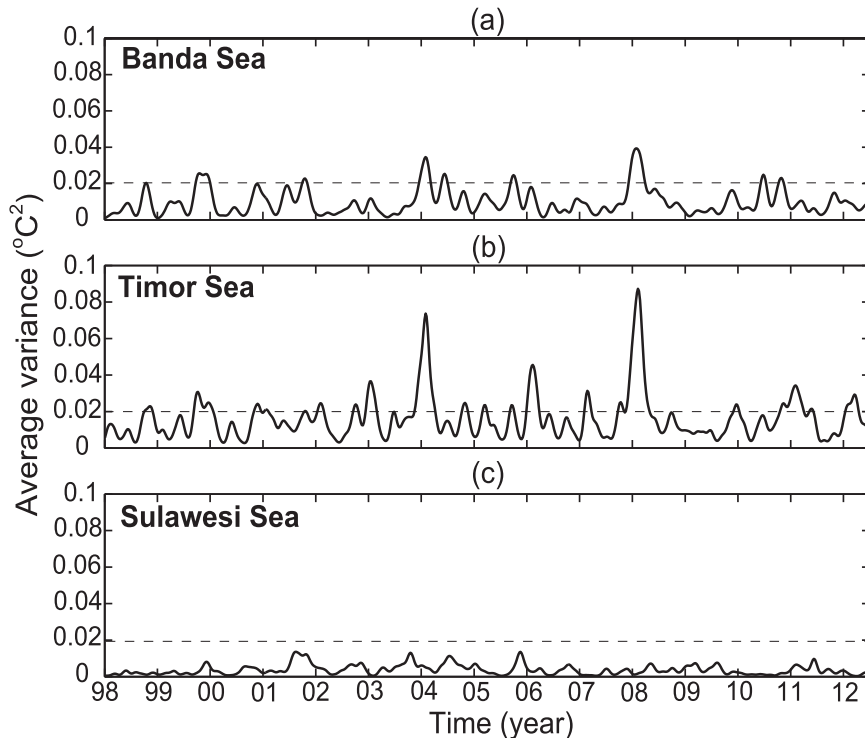


FIG. 4. Time series of SST variances varying at periods of 28–56 days in the (a) Banda Sea, (b) Timor Sea, and (c) Sulawesi Sea. Each time series is obtained from a wavelet analysis to spatially averaged SST data within the dashed box shown in Fig. 1a. Dashed horizontal line denotes the 95% significance level.

variation attributed to the MJO explains a substantial amount of intraseasonal SST variances in the Banda and Timor Seas.

A simple slab model, expressed in (3), quantitatively shows that intraseasonal SST variations in the Banda and Timor Seas are largely forced by surface heat flux. The model SST explains about 69% ($r = 0.83$) of the observed SST variability at intraseasonal time scales in the Banda Sea, while the model can predict almost 78% ($r = 0.88$) of the observed intraseasonal SST variation in the Timor Sea (Figs. 5a,b). The model results suggest that surface heat flux may account for about three-quarters of the total surface mixed layer heat budget variability at intraseasonal time scales in the Banda and Timor Seas.

Probability distributions of the model SST standard deviation during DJF closely resemble that of the observations, whereas the distributions for the JJA period indicate that the model underestimates the intraseasonal SST amplitude (Figs. 5c,d). Figures 5c,d also show that distributions of the model intraseasonal SST in the Banda and Timor Seas reveal larger amplitude during DJF than JJA, consistent with observations. Shallower mixed layer depth during DJF likely explains

the increased amplitude of intraseasonal SST during that period in the Banda and Timor Seas. Figure 6 demonstrates that intraseasonal SST variations do not solely follow that of surface heat flux but are also controlled by mixed layer depth. For example, the model intraseasonal SST variability exhibits a continuously decreasing trend from January to June, although the amplitude of intraseasonal surface net heat flux increases from April to June (Figs. 6a,b). The sustained attenuation of intraseasonal SST variability from April to June is partly controlled by the mixed layer depth, which gets deeper over the same period (Fig. 6c). Deeper thermocline, which potentially dampens the role of ocean processes in modulating the mixed layer heat content, might also contribute to stronger surface flux impact on SST during DJF in the Banda and Timor Seas. Gordon and Susanto (2001) suggested that less energetic upwelling explains deeper thermocline during DJF in the Banda Sea.

Our slab ocean model results for the Timor Sea are similar to those of Vialard et al. (2013), who investigated intraseasonal SST variability in the northwestern Australian basin (NWAB), which is to the southwest of our Timor Sea domain. Nevertheless, their slab ocean model

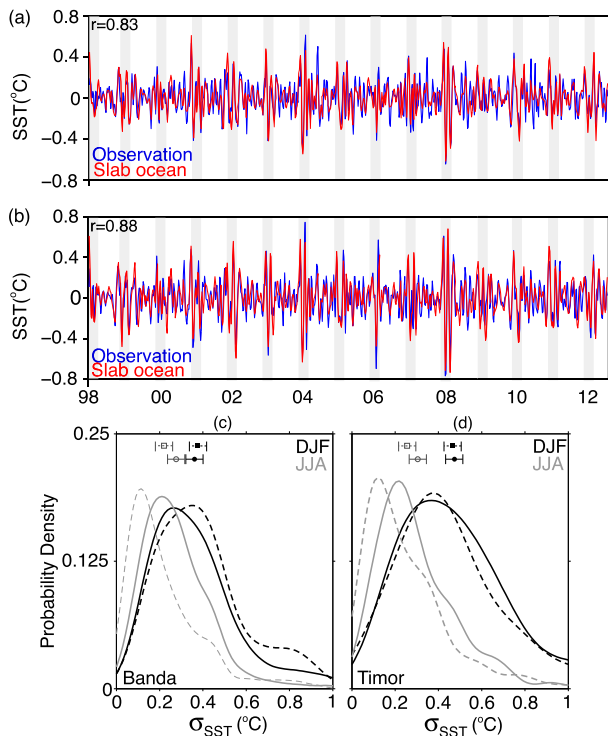


FIG. 5. Time series of the observed (blue) and slab ocean model (red) intraseasonal SST in the (a) Banda Sea and (b) Timor Sea. Gray bars mark the DJF period. Probability density functions of the observed (solid curves) and model (dashed curves) standard deviation of intraseasonal SST in the (c) Banda Sea and (d) Timor Sea. Black (gray) curve indicates the distribution for the DJF (JJA) period. Colored circle (rectangular) denotes the mean of the observed (model) standard deviation of intraseasonal SST.

overestimates the intraseasonal SST amplitude during JJA, while our model underestimates the observation during JJA in the Timor Sea (Fig. 5d).

We have shown that surface heat flux is the primary driver of intraseasonal SST variability in the Banda and Timor Seas. Some studies suggested that the intraseasonal surface flux variability over the Indo-Pacific region is associated with the MJO (Duvel and Vialard 2007; Drushka et al. 2012). To further illustrate the relationship between intraseasonal SST features and the MJO over the Banda and Timor Seas, we investigate both precipitation and OLR variability, which may reflect atmospheric tropical convection variability associated with the MJO.

The significance of intraseasonal precipitation and OLR is obtained through computing a ratio of intraseasonal signal to other signals using (1), and the ratio demonstrates that intraseasonal precipitation and OLR variability is significant over the Banda and Timor Seas. Intraseasonal variability explains about 20%–40% and 40%–50% of OLR and precipitation

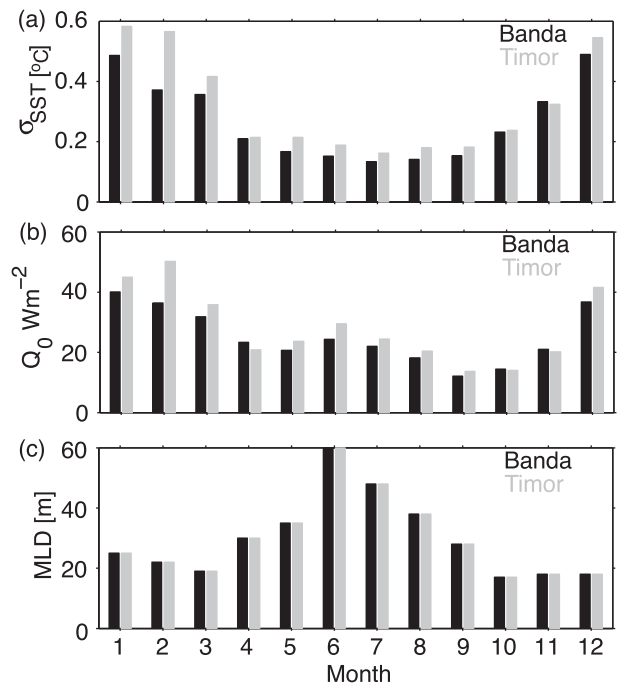


FIG. 6. Seasonal variation of (a) the slab ocean model intraseasonal SST standard deviation, (b) the shortwave radiation flux standard deviation, and (c) the mixed layer depth in the Banda (black) and Timor (gray) Seas.

total variances, respectively (not shown). The average standard deviation of intraseasonal OLR and precipitation over the Banda and Timor Seas varies between 16 and 20 W m^{-2} and 0.15 and 0.22 mm h^{-1} , respectively (not shown).

Oscillations at periods of 35–42 characterize OLR in the Banda and Timor Seas and precipitation over the Timor Sea (Figs. 7a,b,d). Meanwhile, a broader spectral peak with periods of 35–49 days characterizes the precipitation over the Banda Sea (Fig. 7c). Moreover, intraseasonal OLR variability over the Banda and Timor Seas demonstrates seasonality—that is, larger OLR variance (18–25 W m^{-2}) during DJF than during JJA (6–10 W m^{-2}) (Fig. 8a). Similar to OLR, the average precipitation during DJF, varying between 0.28 and 0.31 mm h^{-1} , is larger than that during JJA, varying between 0.2 and 0.28 mm h^{-1} (Fig. 8b). This is consistent with the result of Zhang and Dong (2004) for the broader Indo-Pacific region, suggesting that MJO activity is stronger during DJF than JJA. Furthermore, intraseasonal OLR and precipitation signals over the Indonesian Seas exhibit eastward propagation along the equator with a phase speed of 5–8 m s^{-1} , which is another documented MJO characteristic across the tropics (Zhang 2005). We conclude that strong intraseasonal activities across the Indonesian Seas are

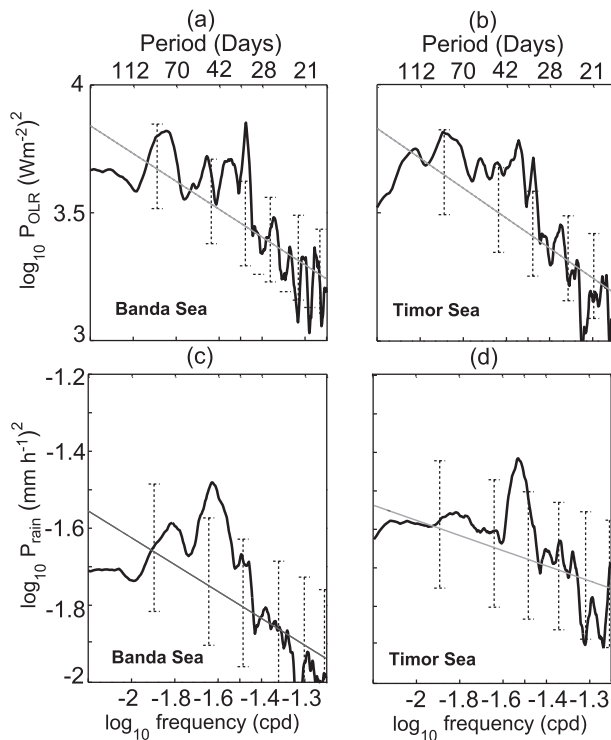


FIG. 7. Power spectrum estimates of (a),(b) OLR and (c),(d) precipitation over the Banda and Timor Seas. Each spectrum estimate is an average over a region bounded by the dashed box shown in Fig. 1a. Gray line and error bars denote the red noise and 80% significance level, respectively.

consistently observed in SST, OLR, and precipitation with similar characteristics.

To quantify the relationship between SST and both OLR and precipitation at intraseasonal time scales, we apply a coherence method. The coherence analysis shows that the dominant intraseasonal SST, OLR, and precipitation in the Banda and Timor Seas are coherent with r^2 varying between 0.5 and 0.7 (Figs. 9a,c). Furthermore, the phase lag of the coherent signals suggests that both OLR and precipitation lead SST by 7–14 days (Figs. 9b,d), which implies that atmosphere processes plays an important role in controlling the intraseasonal SST of the Banda and Timor Seas.

2) SULAWESI SEA

As discussed in section 3a, Sulawesi Sea SST exhibits strong intraseasonal variations with different characteristics observed from the Banda and Timor Seas. The slab-model-derived SST indicates that surface heat flux predicts less than 40% ($r = 0.6$) of the observed intraseasonal SST variability in the Sulawesi Sea (Fig. 10a). The amplitude of the model intraseasonal SST variability appears smaller than that of the observed intraseasonal

SST variability (Fig. 10b). The model shows that the surface heat flux–forced intraseasonal SST does not show seasonality, and neither does the surface net heat flux (Figs. 10b,c). Moreover, the model intraseasonal SST fluctuation follows the surface net heat flux variation, exemplifying the absence of seasonality in the mixed layer depth (Figs. 10b–d). Because the model and observed intraseasonal SSTs show a rather weak correlation and nonseasonal nature, we argue that intraseasonal SST variability in the Sulawesi Sea is derived from an ocean process and/or atmospheric process unrelated to the MJO. To identify other factors other than surface heat flux that might force intraseasonal SST anomalies in the Sulawesi Sea, we examine intraseasonal variation in winds and SLA.

The first complex empirical orthogonal function (CEOF) mode of average 2° – 4° N intraseasonal wind stress along 117° – 125° E over January 1998–mid-2012 reveals that the 20–30-day and 50–60-day variations characterize intraseasonal wind stress anomalies in the Sulawesi Sea. The reconstructed zonal wind stress data using the leading mode, containing about 80% of intraseasonal wind stress anomalies, clearly show that oscillations at 20–30 days and 50–60 days dominate intraseasonal zonal wind stress variability (Fig. 11a). The data also indicate that intraseasonal zonal wind stress does not show eastward propagation over the Sulawesi Sea, which rules out the link between wind stress in the Sulawesi Sea and the MJO. We show only the zonal component of wind stress anomalies because the dominant oscillation’s signature is weak in the meridional component.

We test a plausible relationship between SST and winds in the Sulawesi Sea by applying a coherence method to the data. Coherence analysis between SST and zonal wind stress time series, basin averaged over the Sulawesi Sea, indicate that both SST and zonal wind stress are coherent across the periods of 20–30 days with the squared coherence of 0.5, significant above the 95% significance level (Fig. 11b). The phase lag of the coherent oscillations indicates that zonal wind stress leads SST by about 3 days (Fig. 11c). We thus suggest that the zonal wind stress oscillations at 20–30 days might induce a fraction of the total intraseasonal SST variances in the Sulawesi Sea.

Eddies dominate ocean processes at intraseasonal time scales in the Sulawesi Sea (Qiu et al. 1999; Masumoto et al. 2001; Pujiana et al. 2009). Using a numerical model, Qiu et al. (1999) and Masumoto et al. (2001) proposed that barotropic instability-generated vortical motions in southern Mindanao largely contribute to intraseasonal variability in the Sulawesi Sea. Pujiana et al. (2009) argued that the eddies oscillate at

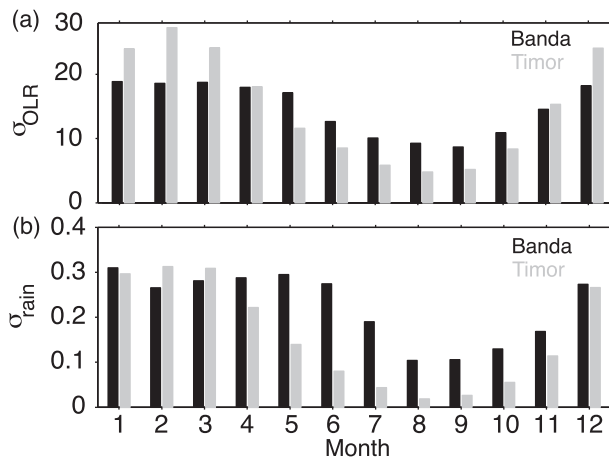


FIG. 8. Seasonal variation of the intraseasonal (a) OLR and (b) precipitation standard deviation in the Banda Sea (black) and Timor Sea (gray). The seasonal variation at each sea is an average over a region bounded by the dashed box shown in Fig. 1a.

around 50–60 days and propagate westward with a speed of the first baroclinic mode of a Rossby wave. The eddies' signatures are evident across the upper thermocline in the Makassar Strait, to the southwest of the

Sulawesi Sea (Pujiana et al. 2012). Eddy motions therefore potentially induce intraseasonal SST variability in the Sulawesi Sea.

To gauge the likelihood of eddies in generating SST in the Sulawesi Sea, we will show the correlation between eddy-induced SLA and SST, which has not been addressed in previous studies. A CEOF analysis to the intraseasonal SLA along 118°–125°E (averaged across 2°–5°N) reveals that the first CEOF mode accounting for 60% of the SLA variability signifies an eddy characteristic, which is westward propagation. The reconstructed intraseasonal SLA attributed to the first CEOF mode clearly demonstrates westward-propagating SLA at a speed of 0.2–0.4 m s⁻¹ (Fig. 12a), which is within the speed range for a baroclinic Rossby wave and consistent with the findings of Qiu et al. (1999), suggesting that eddies in the Sulawesi Sea are constrained by the baroclinic Rossby wave dynamics. A snapshot of intraseasonal SLA in 17 October 2007 in the Sulawesi Sea reveals a sea surface low and high, likely attributed to cyclonic and anticyclonic eddies, respectively, propagating westward (Fig. 12b). The propagating feature in SLA appears periodically at 50–60-day time scales (Fig. 12a).

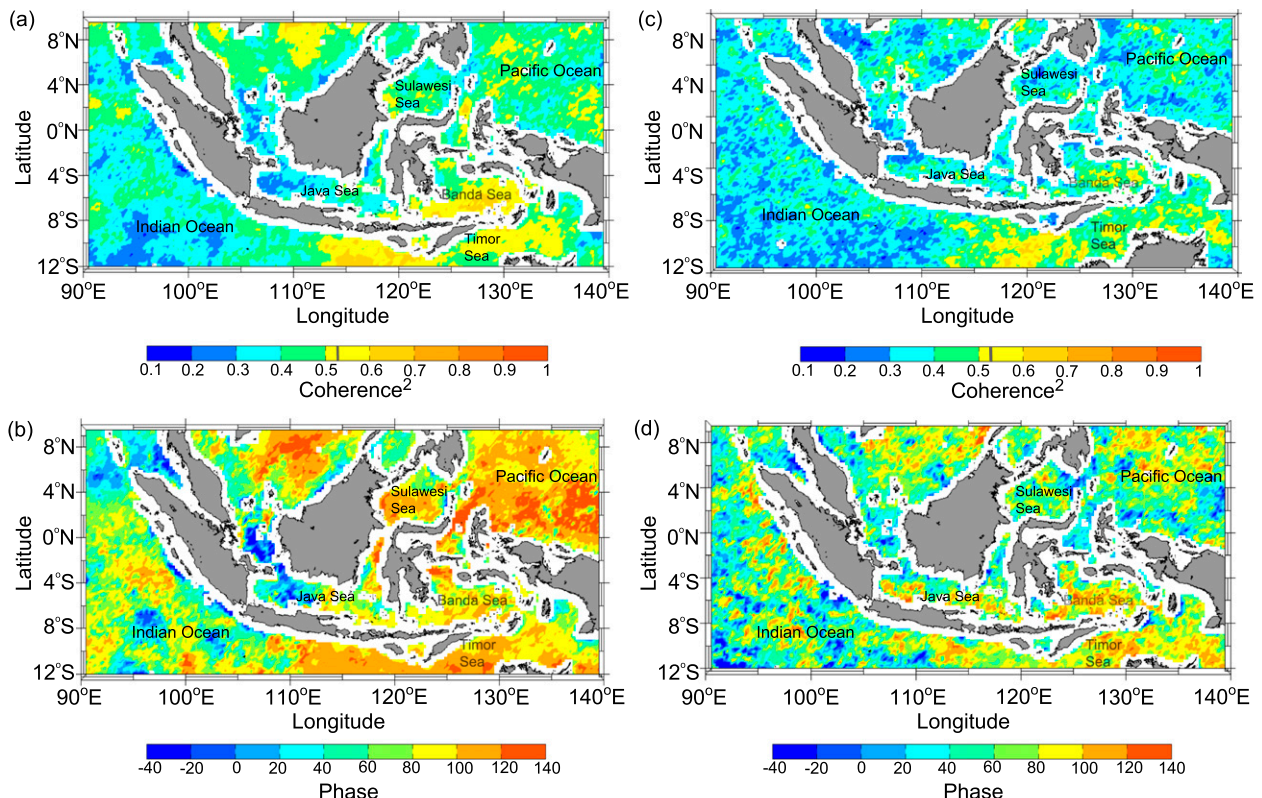


FIG. 9. Coherence between (a),(b) SST and OLR and between (c),(d) SST and precipitation at intraseasonal time scales across the Indonesian Seas. (a),(c) Squared coherence amplitude and (b),(d) phase difference averaged across a period of 28–56 days. A positive phase difference value indicates that OLR/precipitation leads SST. Vertical gray line on the squared coherence color bar marks the 95% significance level.

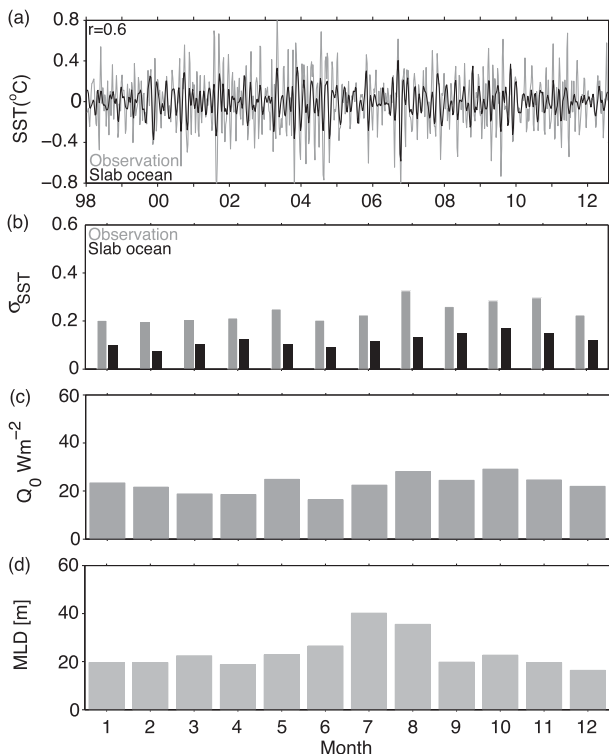


FIG. 10. (a) Time series of the observed (gray) and slab ocean (black) model intraseasonal SST in the Sulawesi Sea. Seasonal variation of the standard deviation of intraseasonal (b) SST and (c) shortwave radiation flux in the Sulawesi Sea. (d) Seasonal variation of the basin-averaged mixed layer depth in the Sulawesi Sea. The data shown in (a),(b),(c), and (d) are basin averaged within the dash box shown in Fig. 1a.

The 50–60-day signal also characterizes the first CEOF mode of intraseasonal SST at the same location, for which the CEOF mode accounts for 73% of the total intraseasonal SST variability. Unlike the SLA, the 60-day SST signal does not appear to propagate westward at a speed range of $0.2\text{--}0.4\text{ ms}^{-1}$. The signal occurs almost instantaneously across the longitudes in the Sulawesi Sea. Although the dominant intraseasonal SST and SLA variability do not demonstrate a westward-propagating feature consistently at the same speed, they are statistically coherent (Fig. 12c). The basin-averaged phase lag of the coherent oscillations indicates that SLA leads SST by about 8 days (Fig. 12d). We thus suggest that the eddy motions at 50–60 days might induce a fraction of the total intraseasonal SST variances in the Sulawesi Sea.

4. The Banda Sea SST response to 2007/08 MJO events

We have shown that the dominant SST variations at intraseasonal time scales in the Banda and Timor Seas

share distinct characteristics attributed to the MJO. The MJO surface heat flux contributes substantially to force intraseasonal SST in the Banda and Timor Seas, where the MJO-induced intraseasonal SST explains about 69%–78% of the total observed intraseasonal SST variability, as inferred from the slab ocean model results (Figs. 5a,b). The contribution of the MJO surface heat flux to force the mixed layer heat budget variability varies as a function of time. A cross-wavelet transform of the slab-ocean-model-derived SST and observed SST at intraseasonal time scales in the Banda Sea shows that the SST response to surface net heat flux varies with time: stronger during DJF and weaker during JJA (Fig. 13b). This indicates that intraseasonal SST variability is dominated by surface flux variations in DJF, but other processes come into play in JJA. In addition to seasonal variation, the impact of surface heat flux on intraseasonal SST in the Banda Sea also exhibits interannual variations. Intraseasonal surface heat flux–forced SST is statistically correlated to the Niño-3.4 index (Fig. 13a), with $r = -0.47$, indicating a significant correlation between the MJO-forced SST and the ENSO state. The impact of intraseasonal surface flux on intraseasonal SST appears stronger during neutral and La Niña years (e.g., 2004 and fall 2007–spring 2008), while it is weaker during El Niño phases (e.g., late 2006) (Fig. 13). Over the period of January 1998–mid-2012, the correlation between the model and observed SST is strongest during November 2007–February 2008 (ND07/JF08) (Fig. 13b). Furthermore, the time series of intraseasonal Banda Sea SST variances between January 1998 and mid-2012 is observed largest during ND07/JF08 (Fig. 4). A more detailed discussion on how the MJO surface flux projects its signature on SST over the Banda Sea during ND07/JF08 is now investigated. We here solely focus our analysis on the Banda Sea, not on the Timor Sea, because intraseasonal variability features observed in both the Banda and Timor Seas are strongly correlated.

To understand the MJO–SST coupling across the Banda Sea, the relationship between surface heat flux attributable to MJO life cycle and SST needs to be examined. Some studies suggest that surface heat flux attributed to MJO is the primary driver for SST variability (Shinoda et al. 1998; Duvel et al. 2004; Vialard et al. 2013). An MJO life cycle involves an active phase preceded by a suppressed phase. Reduced shortwave radiation due to strong convection and intense evaporative cooling driven by westerly wind bursts mark the MJO active phase (Shinoda et al. 1998).

Analyses of SST response to MJO are focused on two strong MJO events during ND07/JF08. We extend our analysis from the Indonesian Maritime Continent to a

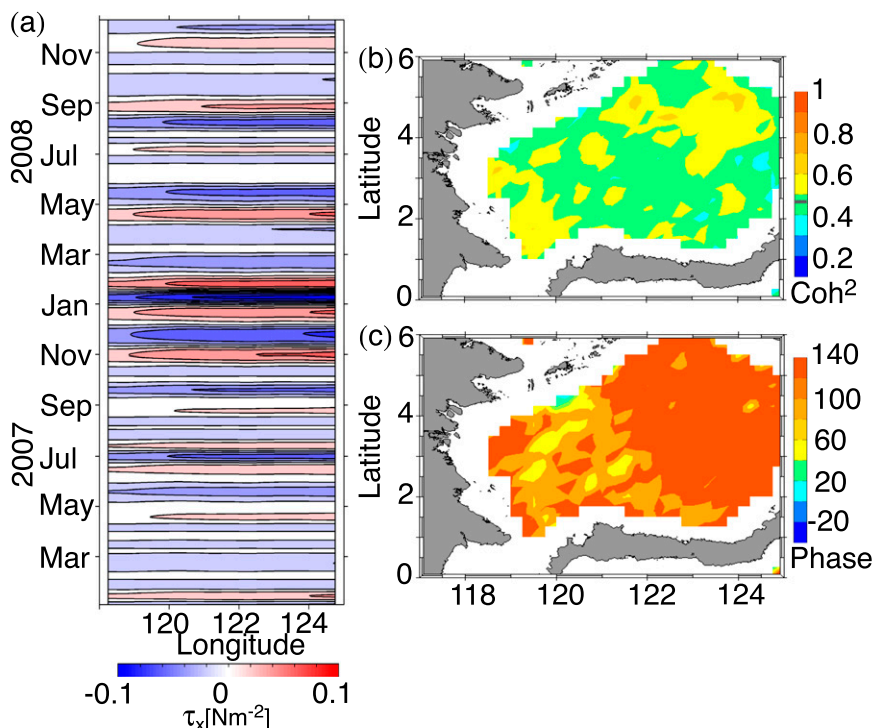


FIG. 11. (a) Time–longitude plot of the reconstructed intraseasonal zonal wind stress over the Sulawesi Sea. The leading CEOF mode of the zonal wind stress data along 118° – 125° E and averaged over 2° – 4° N observed during January 1998–mid-2012 is used to obtain the reconstructed data. The data during 2007/08 are arbitrarily selected. Coherence between zonal wind stress and SST in the Sulawesi Sea. (b) Squared coherence and (c) phase lag averaged across a period band of 20–30 days. Horizontal black line on the squared coherence color bar marks the 95% significance level.

broader region including the tropical Indian Ocean in order to examine the MJO evolution from the Indian Ocean to Pacific Ocean (Fig. 14a). Vialard et al. (2008), using data from a mooring located in the Seychelles–Chagos thermocline ridge (SCTR), examined the impact of the ND07/JF08 MJO on SST in the tropical Indian Ocean. They showed that strong SST variability in the SCTR region during the ND07/JF08 period was correlated with the MJO, whose air–sea heat flux dominated the upper-ocean heat budget.

Our analyses indicate that a series of MJO events propagating eastward at a phase speed varying between 4 and 9 m s^{-1} is evident in OLR and zonal wind stress data during ND07/JF08 (Figs. 14a,b). Each MJO event appears in OLR as a pair of positive and negative OLR phases, respectively, where a positive phase indicates larger OLR or less atmospheric convection and a negative phase implies colder cloud tops or more atmospheric convection (Fig. 14a). The positive OLR (MJO suppressed phase) precedes the negative OLR (MJO active phase), and it takes about 1 month for each pair of propagating OLR to complete a cycle of

positive and negative phases. Eastward propagation of MJO convective clouds along its path across the tropics also manifests in the wind variation. For the ND07/JF08 MJO sequence, the suppressed MJO phase was characterized by calm winds while the active MJO phase was marked with westerly wind bursts (Fig. 14b).

The eastward-propagating feature during ND07/JF08 was consistently observed from the tropics of the central Indian Ocean to that of the western Pacific Ocean (Figs. 14a,b). The Wheeler and Hendon (2004) real-time multivariate MJO (RMM) index during this particular period links the pairs of eastward-propagating OLR and wind stress to two MJO events (Figs. 14d,e). The index, OLR, and wind stress are in agreement that the first MJO active phase (negative OLR and strong wind stress) occurred and propagated across the Indonesian Maritime Continent from mid-December 2007 to early January 2008, while the second MJO active event followed up and prevailed across the region in early February 2008 (Figs. 14a,b,d,e). Each of the MJO active phases during the period of ND07/JF08 was preceded

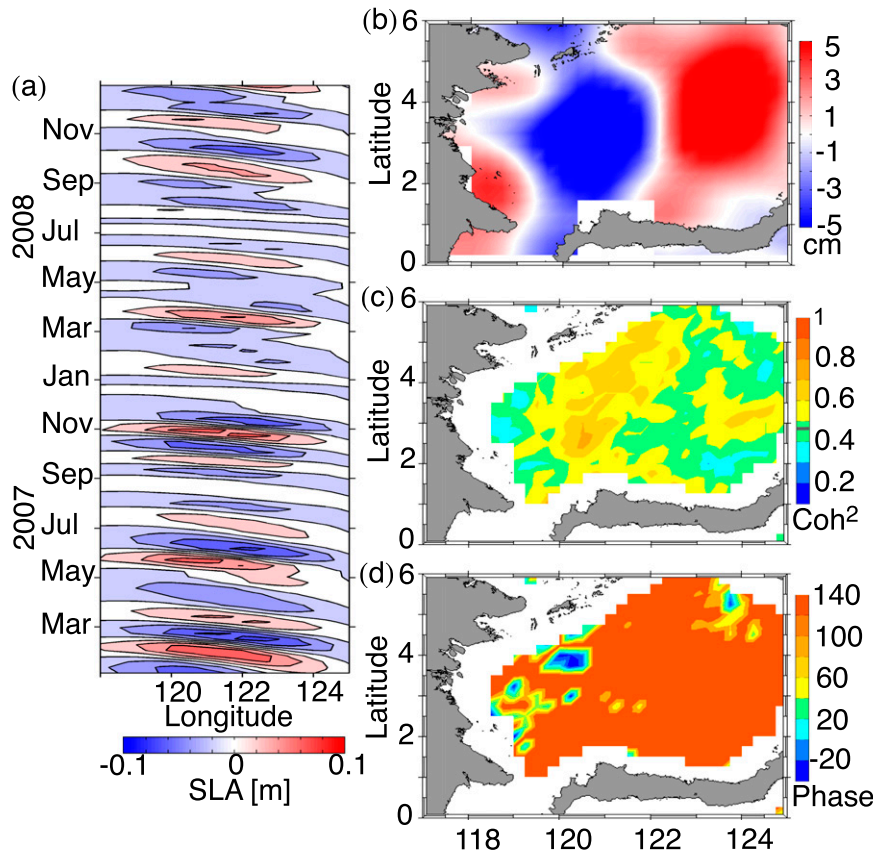


FIG. 12. (a) Time–longitude plot of the reconstructed intraseasonal SLA in the Sulawesi Sea. The leading CEOF mode of the SLA data along 118°–125°E and averaged over 2°–4°N observed during January 1998–mid-2012 is used to obtain the reconstructed data. The data during 2007/08 are arbitrarily selected. (b) A snapshot of intraseasonal SLA over the Sulawesi Sea on 17 October 2007. Coherence between SLA and SST in the Sulawesi Sea. (c) Squared coherence and (d) phase lag averaged across a period band of 20–30 days. Horizontal gray line on the squared coherence color bar marks the 95% significance level.

by a suppressed MJO phase marked by positive OLR (reduced atmospheric convection) and calm winds prevailing across the Maritime Continent. Comparing the time evolution of OLR and RMM index, we find that the two MJO events observed during the period of ND07/JF08 differ in strength, with the first MJO displaying a stronger signature (Figs. 14a,d,e).

The MJO passages propagating from the Indian Ocean to the Pacific Ocean across the Maritime Continent as indicated by OLR and wind stress data are projected in the intraseasonal SST warming and cooling episodes. The Banda Sea responds to passages of positive (negative) OLR and calm (westerly) winds during the ND07/JF08 MJO events by warming and cooling the SST, respectively (Fig. 14c). Moreover, the eastward propagation observed in OLR and wind stress associated with MJO is also evident in SST with a phase speed of 4–5 m s⁻¹.

Since OLR, wind stress, and SST reveal similar features, one of which is eastward propagation, we conclude that intraseasonal SST fluctuations within the Banda Sea (and Timor Sea) are related to the MJO. The evolution of the first MJO propagating across the Maritime Continent during ND07/JF08 and how the SST responds to that event in the Banda Sea can be seen in Figs. 15a–c. The onset of the first weak convective, passive phase was marked by positive OLR reaching the Banda Sea in late November 2007 and then followed by weak easterlies around a week after the positive OLR passed the Banda Sea. The sea surface responds to the passive phase by warming the temperature by about 1°C. After the positive OLR completely passes across the Banda Sea, the propagation of deep convection within the atmosphere marking the active MJO phase reaches the Banda Sea. The convection that we can identify from the negative OLR

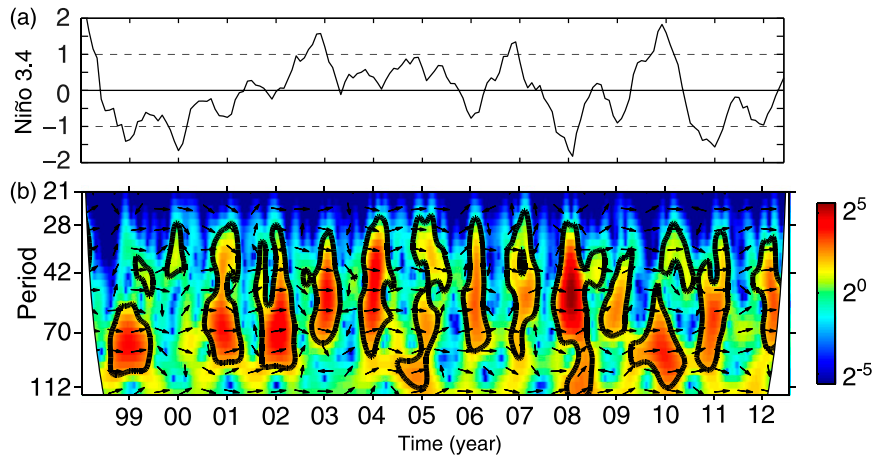


FIG. 13. (a) Time series of the Niño-3.4 index. (b) Cross-wavelet transform between the observed and slab-ocean-model-derived intraseasonal SST in the Banda Sea. The SST data are basin-averaged values within the dashed box shown in Fig. 1a. Solid thick lines denote the 95% significance level. Arrows pointing right indicate that the observed and model SST are in phase.

event is followed by a strong westerly wind burst. The Banda Sea responds to the reduced solar radiation, due to the deep convection, by cooling its SST by about 2°C (Figs. 15d–f).

The slab-model-derived SST variability shows a good agreement with the observed SST variability at intraseasonal time scales in Banda Sea over January 1998–mid-2012 (Fig. 5a). The correlation between the model and observed SST variability improves during ND07/JF08 with the former explains about 90% of the later (Fig. 16a). Moreover, Fig. 14 displays a strong correspondence between SST, OLR, and wind stress during the MJO phases of ND07/JF08. We thus propose that air–sea heat flux driven by atmospheric forcing associated with the MJO phases is more dominant than ocean mixed layer processes in governing intraseasonal SST variation during ND07/JF08.

The reanalysis data indicate that the net surface heat flux during ND07/JF08 was mostly controlled by solar radiation and latent heat flux (Figs. 16b,c). Intraseasonal shortwave and latent heat flux combined contributes about 98% of intraseasonal surface net heat flux variability (Fig. 16c). A combination of suppressed evaporative cooling due to calm winds and shortwave radiation during the first passive MJO phase from mid-November to mid-December 2007 resulted in an accumulated net heat flux of 758 W m^{-2} , which warmed SST by $+1.1^{\circ}\text{C}$ (Figs. 16a,b). The ensuing active MJO phase characterized by attenuated shortwave radiation and amplified latent heat flux to the atmosphere driven by a strong westerly wind burst reaching its maximum strength in early January 2008 resulted in an accumulated net heat flux into the atmosphere of 1424 W m^{-2} , which cooled

SST by -2.1°C (Figs. 16a,b). The overall cooling effect registered during the first MJO event is controlled by a larger heat flux into the atmosphere during the MJO active phase than that accumulated by the ocean during the MJO passive phase. By contrast, the second MJO-induced intraseasonal SST warming of 0.2°C , the amount of heat flux into the ocean registered during the MJO passive phase through early–late January 2008, was slightly larger than the heat flux released to the atmosphere during the MJO active phase in February 2008 (Figs. 16a,b). The ocean gained about 1534 W m^{-2} of net heat flux, which increased intraseasonal SST by 2°C , over the MJO passive phase period. Moreover, the ocean lost about 1402 W m^{-2} , cooling intraseasonal SST by 1.8°C , during the MJO active phase period.

5. Summary and discussion

a. Summary

Satellite-derived SST data, which extend from 1998 to mid-2012, reveal that intraseasonal variability explains about 18% of SST total variances over the Indonesian Seas. The largest intraseasonal contribution to the total nonseasonal SST variances are observed in the Banda, Timor, and Sulawesi Seas, with energy peaks centered at 35 days in the Banda and Timor Seas and at 25 and 56 days in the Sulawesi Sea.

The intraseasonal SST signals in the Banda and Timor Seas exhibit larger seasonal variation during the northern winter months (DJF) relative to the summer months (JJA). The standard deviation of intraseasonal SST anomalies varies between 0.6° and 0.7°C during DJF and

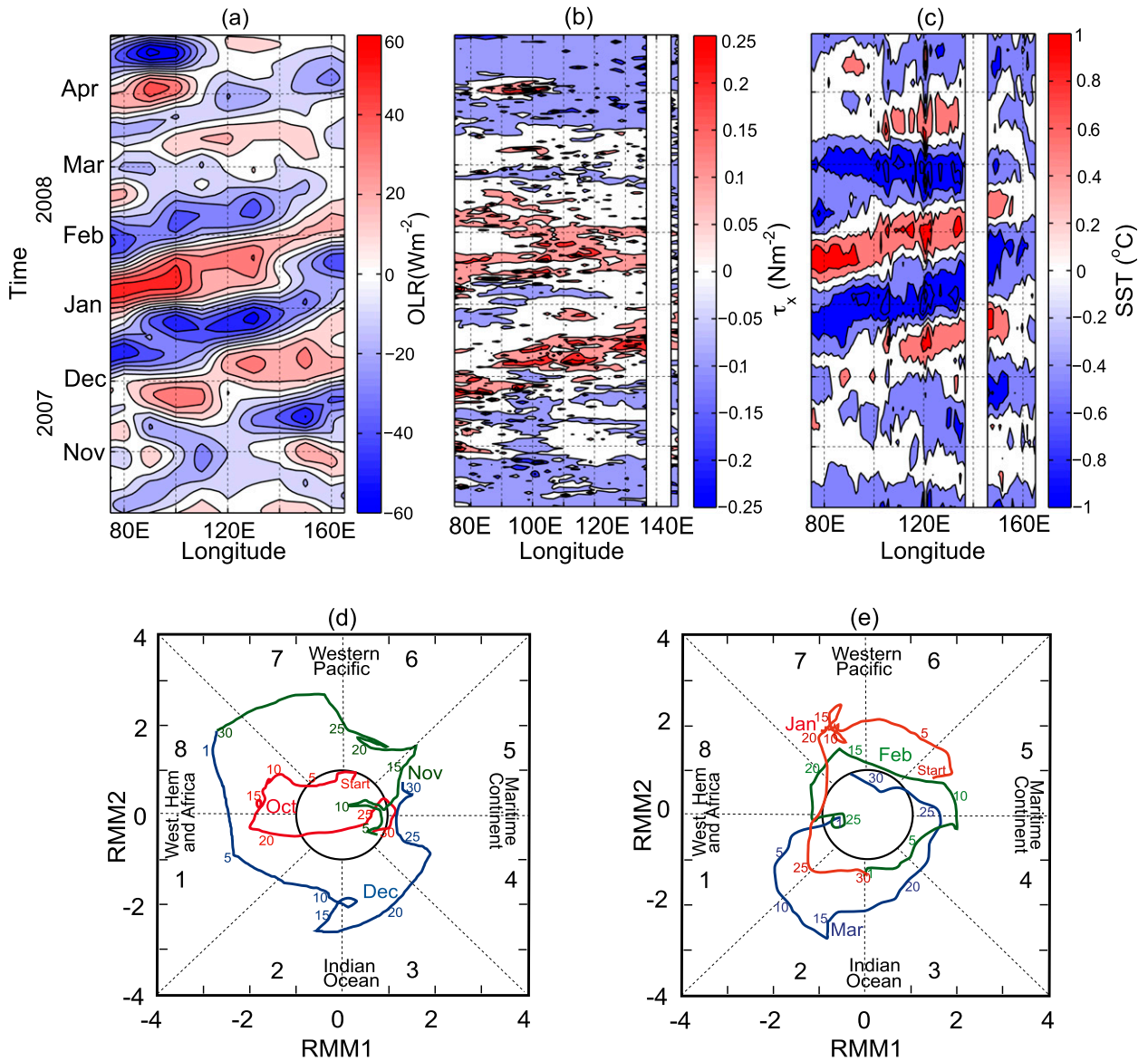


FIG. 14. Time–longitude plots of intraseasonal (a) OLR, (b) zonal wind stress, and (c) SST during late fall 2007–spring 2008, averaged across 4°–7.5°S. RMM index during (d) October–December 2007 and (e) January–March 2008.

0.2° and 0.3°C during JJA. MJO surface heat flux accounts for significant variance of the coherent intraseasonal SST in the Banda and Timor Seas. The slab-ocean-model-derived SST variation quantitatively demonstrates that surface net heat flux may explain 78% of intraseasonal SST variability within the Timor Sea, while it accounts for 69% of intraseasonal SST in the Banda Sea. The MJO-forced intraseasonal SST in the Banda and Timor Seas also shows variations on interannual time scales.

Over the period of January 1998–mid-2012, the magnitudes of intraseasonal SST variability in the Banda and Timor Seas are strongest between November 2007 and February 2008, during which two strong MJO events

were recorded. During those MJO passages, intraseasonal SST in the Banda Sea responds to the MJO suppressed and active phases by warming and cooling, respectively. The SST warms during the suppressed MJO phase (positive OLR) as a result of weaker winds and more shortwave radiation, with increased net surface heat flux into the ocean. More convective clouds (negative OLR), stronger westerly winds, reduced shortwave radiation, and increased evaporation lead to more heat transferred to the atmosphere, cooling the SST during the MJO active phase. The dominance of surface heat flux associated with the MJO in forcing intraseasonal SST is evident from observed eastward propagation in SST.

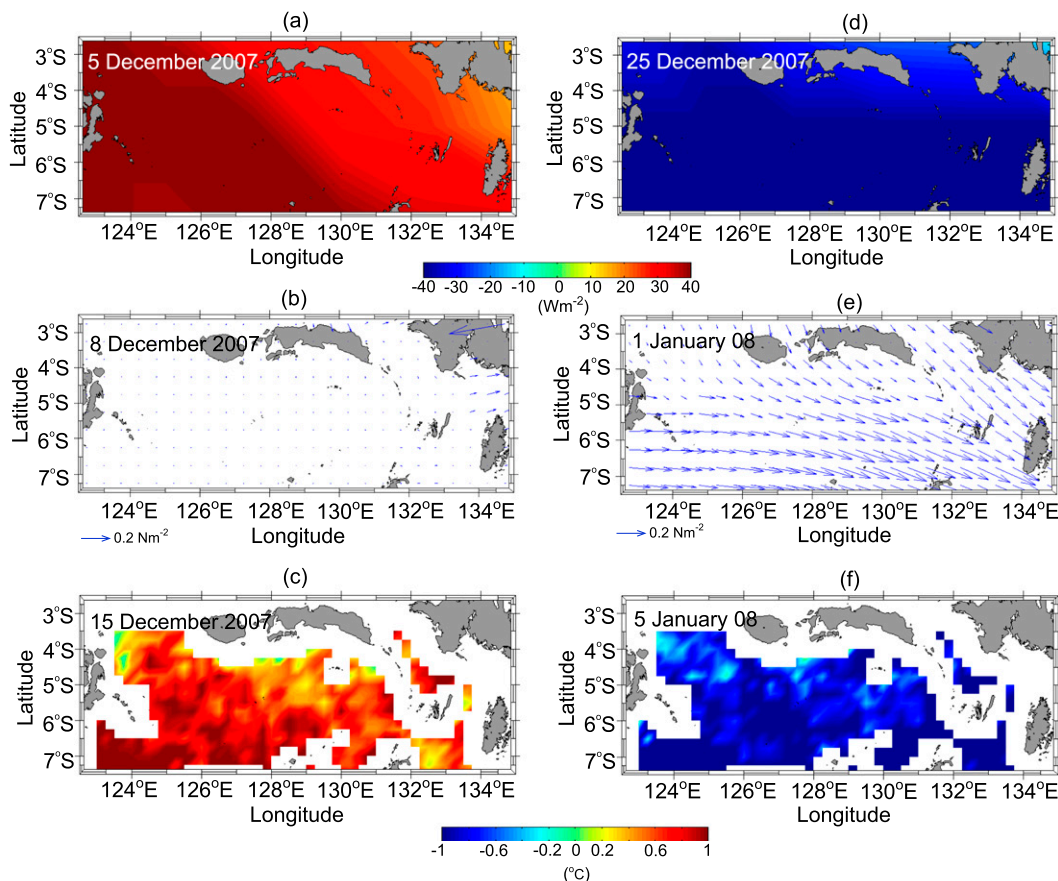


FIG. 15. Snapshots of intraseasonal OLR, wind stress, and SST over the Banda Sea attributed to (a)–(c) a passive MJO phase during early–mid-December 2007 and (d)–(f) an active MJO phase during late December 2007–early January 2008. The dates are selected to represent the period of maximum (minimum) OLR and SST and of weakest (strongest) wind during the MJO suppressed (active) phase.

The intraseasonal SST variability in the Sulawesi Sea is characterized by dominant oscillations of 50–60 and 20–30 days, and it does not demonstrate significant correlation with intraseasonal SST in the Banda and Timor Seas. The slab ocean model predicts less than 40% of intraseasonal SST variability in the Sulawesi Sea. Unlike in the Banda and Timor Seas, intraseasonal SST and surface heat flux in the Sulawesi Sea do not exhibit seasonal fluctuations, a characteristic that couples MJO surface heat flux to intraseasonal SST variability. In addition to surface flux, a combination of eddy- and wind-induced SST may contribute to a considerable fraction of intraseasonal SST variance in the Sulawesi Sea. Eddy motion, signifying westward propagation at a baroclinic Rossby wave speed of $0.2\text{--}0.4\text{ m s}^{-1}$ in intraseasonal SLA variability, is coherent with the dominant intraseasonal SST variability with $r^2 = 0.45$ at periods of 50–55 days. We also demonstrate that the 20–30-day zonal wind stress variability is coherent with that of SST in the Sulawesi Sea with $r^2 = 0.5$. This dominant period

band of the zonal wind stress does not exhibit eastward propagation, dissociating it from MJO forcing.

b. Discussion

The intraseasonal SST response in the Banda and Timor Seas to MJO surface flux is amplified during DJF and attenuated during JJA. The slab ocean model reveals the role of the mixed layer in the relationship of intraseasonal SST seasonal variability to surface heat flux. During DJF in the Banda and Timor Seas, a larger air–sea net heat flux, coupled with reduced wind and greater rainfall, results in a more buoyant mixed layer depth that isolates the surface water from the cooler subsurface stratum inhibiting the role of ocean processes in governing the mixed layer heat content variability.

The signature of the surface heat flux–induced intraseasonal SST in the Banda and Timor Seas displays variation not only at the seasonal time scale but also at the interannual time scale. The surface heat flux imprint on SST tends to be greater during neutral and La Niña years,

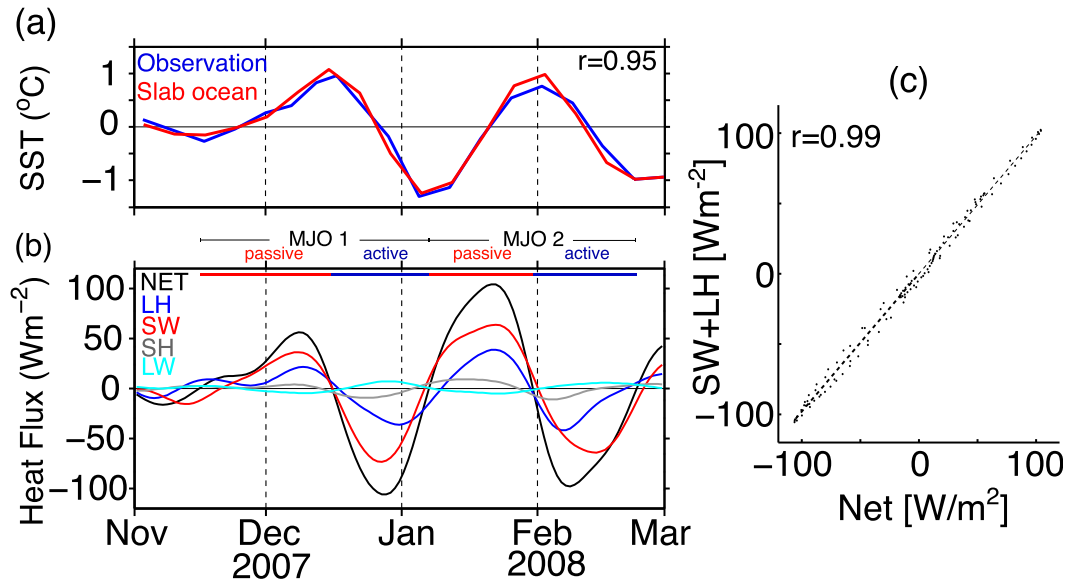


FIG. 16. (a) Time series of intraseasonal SST from observations (blue) and slab ocean model (red) in the Banda Sea. (b) Time series of intraseasonal net (black), shortwave radiation (red), latent (blue), sensible (gray), and longwave (cyan) heat fluxes over the Banda Sea. Positive value indicates heat flux into the ocean. (c) Scatterplot of net heat flux and sum of shortwave and latent heat fluxes in the Banda Sea. Dashed line denotes a line fit with a slope of 0.99. Horizontal red and blue bars indicate the active and passive phase respectively attributed to the MJO-1 and MJO-2 passages. Time series in (a), (b), and (c) are basin-averaged values in the Banda Sea within the box indicated in Fig. 1a.

when the mixed layer is more buoyant, with weaker SST response to surface heat flux during El Niño. The ENSO signal may indicate a response to the reduced rainfall during El Niño when the mixed layer is denser, increasing the role of ocean processes in regulating the mixed layer heat budget variability at intraseasonal time scales.

The role of ocean processes is likely to be larger in the Banda Sea than in the Timor Sea, as surface heat flux explains a smaller fraction of intraseasonal SST variability within the Banda Sea. Major ocean processes that may contribute to SST variations in the Banda Sea are Ekman-driven upwelling and downwelling at seasonal and interannual time scales. Gordon and Susanto (2001) reported that the coldest (warmest) SST in the Banda Sea occurs in JJA (DJF). The period of colder (warmer) SST is driven by stronger upwelling (downwelling). The JJA mixed layer is denser than the DJF mixed layer. A more buoyant mixed layer in DJF and during La Niña within the Banda Sea explains the atmospheric heat flux dominance in forcing intraseasonal SST in the Banda Sea during DJF and La Niña, when the ocean processes' effect on SST is reduced.

We find that MJO surface heat flux accounts for significant variance of the coherent intraseasonal SST in the Banda and Timor Seas. The characteristics of OLR, precipitation, and zonal wind stress at intraseasonal time

scales over the Banda and Timor Seas are similar to that of SST and correspond to MJO characteristics (Zhang and Dong 2004; Zhang 2005).

The slab ocean model is relatively simple, and it does not resolve the impact of the sub-monthly surface mixed layer depth variability on intraseasonal SST because we applied monthly climatology in our computation. Our results, however, suggest that the model approximately reproduces observations, delineating the dominant role of intraseasonal surface heat flux in forcing intraseasonal SST, particularly during DJF in the Banda and Timor Seas. Through applying a similar approach, Vialard et al. (2013) found that the slab model provides a good estimate of 79% SST variability at periods of 30–110 days in the NWAB. Moreover, Duvel et al. (2004), Duvel and Vialard (2007), and Drushka et al. (2012) concluded that net surface heat flux anomalies dominate the overall mixed layer heat budget of the Indo-Pacific at intraseasonal time scales. We suggest that oceanic heat flux significantly contributes to SST during the JJA and El Niño periods within the Banda and Timor Seas. To quantify the oceanic heat flux contribution, we would need to examine oceanic parameter measurements such as ocean currents and mixing rates, which are rather limited or nonexistent in our study area.

We have shown that intraseasonal SST in the Banda and Timor Seas is responsive to the MJO, and the response displays interannual variation in which warmer (colder) background SST attributed to La Niña (El Niño) corresponds with stronger (weaker) projection of MJO in SST. Does warmer sea surface during La Niña in the Banda and Timor Seas provide positive feedback to strengthen the MJO signature as it propagates over the Maritime Continent from the Indian Ocean to the western Pacific Ocean? Future studies will explore this important issue.

Acknowledgments. The constructive comments from three anonymous reviewers are greatly appreciated. This research was funded in part under the Cooperative Institute for Climate Application Research (CICAR) Award NA08OAR4320754 from the National Oceanic and Atmospheric Administration, U.S. Department of Commerce. The statements, findings, conclusions, and recommendations are those of the authors and do not necessarily reflect the views of NOAA or the Department of Commerce. The TMI data are produced by Remote Sensing Systems and sponsored by the NASA Earth Science MEASUREs DISCOVER Project. (The data are available at www.remss.com. The RMM and Niño-3.4 SST index can be obtained from <http://cawcr.gov.au/staff/mwheeler/maproom/RMM/RMM1RMM2.74toRealtime.txt> and http://www.esrl.noaa.gov/psd/gcos_wgsp/Timeseries/Data/nino34.long.anom.data, respectively.)

REFERENCES

- Ardizzone, J., R. Atlas, R. N. Hoffman, J. C. Jusem, S. M. Leidner, and D. F. Moroni, 2009: New multiplatform ocean surface wind product available. *Eos, Trans. Amer. Geophys. Union*, **90**, 231, doi:10.1029/2009EO270003.
- de Boyer Montégut, C., G. Madec, A. S. Fischer, A. Lazar, and D. Iudicone, 2004: Mixed layer depth over the global ocean: An examination of profile data and a profile-based climatology. *J. Geophys. Res.*, **109**, C12003, doi:10.1029/2004JC002378.
- Drushka, K., J. Sprintall, S. T. Gille, and I. Brodjonegoro, 2010: Vertical structure of Kelvin waves in the Indonesian Throughflow exit passages. *J. Phys. Oceanogr.*, **40**, 1965–1987, doi:10.1175/2010JPO4380.1.
- , —, —, and S. Wijffels, 2012: In situ observations of Madden–Julian oscillation mixed layer dynamics in the Indian and western Pacific Oceans. *J. Climate*, **25**, 2306–2328, doi:10.1175/JCLI-D-11-00203.1.
- Ducet, N., P.-Y. Le Traon, and G. Reverdin, 2000: Global high-resolution mapping of ocean circulation from TOPEX/Poseidon and ERS-1 and -2. *J. Geophys. Res.*, **105**, 19 477–19 498, doi:10.1029/2000JC900063.
- Duvel, J. P., and J. Vialard, 2007: Indo-Pacific sea surface temperature perturbations associated with intraseasonal oscillations of tropical convection. *J. Climate*, **20**, 3056–3082, doi:10.1175/JCLI4144.1.
- , R. Roca, and J. Vialard, 2004: Ocean mixed layer temperature variations induced by intraseasonal convective perturbations over the Indian Ocean. *J. Atmos. Sci.*, **61**, 1004–1023, doi:10.1175/1520-0469(2004)061<1004:OMLTVI>2.0.CO;2.
- Gordon, A. L., 2005: Oceanography of the Indonesian Seas and their throughflow. *Oceanography*, **18**, 14–27, doi:10.5670/oceanog.2005.01.
- , and R. D. Susanto, 2001: Banda Sea surface-layer divergence. *Ocean Dyn.*, **52**, 2–10, doi:10.1007/s10236-001-8172-6.
- Grinsted, A., J. C. Moore, and S. Jevrejeva, 2004: Application of the cross wavelet transform and wavelet coherence to geophysical time series. *Nonlinear Processes Geophys.*, **11**, 561–566, doi:10.5194/npg-11-561-2004.
- Halkides, D., T. Lee, and S. Kida, 2011: Mechanisms controlling the seasonal mixed-layer temperature and salinity of the Indonesian Seas. *Ocean Dyn.*, **61**, 481–495, doi:10.1007/s10236-010-0374-3.
- Kessler, W. S., 2001: EOF representations of the Madden–Julian oscillation and its connection with ENSO. *J. Climate*, **14**, 3055–3061, doi:10.1175/1520-0442(2001)014<3055:EROTMJ>2.0.CO;2.
- Kida, S., and K. J. Richards, 2009: Seasonal sea surface temperature variability in the Indonesian Seas. *J. Geophys. Res.*, **114**, C06016, doi:10.1029/2008JC005150.
- Liebmann, B., and C. A. Smith, 1996: Description of a complete (interpolated) outgoing longwave radiation dataset. *Bull. Amer. Meteor. Soc.*, **77**, 1275–1277.
- Madden, R. A., and P. R. Julian, 1994: Observations of the 40–50-day tropical oscillation—A review. *Mon. Wea. Rev.*, **122**, 814–837, doi:10.1175/1520-0493(1994)122<0814:OOTDIO>2.0.CO;2.
- Masumoto, Y., T. Kagimoto, M. Yoshida, M. Fukuda, N. Hirose, and T. Yamagata, 2001: Intraseasonal eddies in the Sulawesi Sea simulated in an ocean general circulation model. *Geophys. Res. Lett.*, **28**, 1631–1634, doi:10.1029/2000GL011835.
- McBride, J. L., M. R. Haylock, and N. Nicholls, 2003: Relationships between the Maritime Continent heat source and the El Niño–Southern Oscillation phenomenon. *J. Climate*, **16**, 2905–2914, doi:10.1175/1520-0442(2003)016<2905:RBTMCH>2.0.CO;2.
- Meehl, G. A., 1987: The annual cycle and interannual variability in the tropical Pacific and Indian Ocean regions. *Mon. Wea. Rev.*, **115**, 27–50, doi:10.1175/1520-0493(1987)115<0027:TACAIV>2.0.CO;2.
- Praveen Kumar, B., J. Vialard, M. Lengaigne, V. Murty, and M. McPhaden, 2012: TropFlux: Air–sea fluxes for the global tropical ocean—Description and evaluation. *Climate Dyn.*, **38**, 1521–1543, doi:10.1007/s00382-011-1115-0.
- Pujiana, K., A. L. Gordon, J. Sprintall, and R. D. Susanto, 2009: Intraseasonal variability in the Makassar Strait thermocline. *J. Mar. Res.*, **67**, 757–777, doi:10.1357/002224009792006115.
- , —, E. J. Metzger, and A. L. Field, 2012: The Makassar Strait pycnocline variability at 20–40 days. *Dyn. Atmos. Oceans*, **53**, 17–35, doi:10.1016/j.dynatmoce.2012.01.001.
- , —, and J. Sprintall, 2013: Intraseasonal Kelvin wave in Makassar Strait. *J. Geophys. Res. Oceans*, **118**, 2023–2034, doi:10.1002/jgrc.20069.
- Qiu, B., M. Mao, and Y. Kashino, 1999: Intraseasonal variability in the Indo–Pacific throughflow and the regions surrounding the Indonesian Seas. *J. Phys. Oceanogr.*, **29**, 1599–1618, doi:10.1175/1520-0485(1999)029<1599:IVTIP>2.0.CO;2.
- Qu, T., Y. Du, J. Strachan, G. Meyers, and J. Slingo, 2005: Sea surface temperature and its variability in the Indonesian region. *Oceanography*, **18**, 50–61, doi:10.5670/oceanog.2005.05.
- Salby, M. L., and H. H. Hendon, 1994: Intraseasonal behavior of clouds, temperature, and motion in the tropics. *J. Atmos.*

- Sci.*, **51**, 2207–2224, doi:[10.1175/1520-0469\(1994\)051<2207:IBOCTA>2.0.CO;2](https://doi.org/10.1175/1520-0469(1994)051<2207:IBOCTA>2.0.CO;2).
- Shinoda, T., H. H. Hendon, and J. Glick, 1998: Intraseasonal variability of surface fluxes and sea surface temperature in the tropical western Pacific and Indian Oceans. *J. Climate*, **11**, 1685–1702, doi:[10.1175/1520-0442\(1998\)011<1685:IVOSFA>2.0.CO;2](https://doi.org/10.1175/1520-0442(1998)011<1685:IVOSFA>2.0.CO;2).
- Sprintall, J., A. L. Gordon, A. Koch-Larrouy, T. Lee, J. T. Potemra, K. Pujiana, and S. E. Wijffels, 2014: The Indonesian Seas and their role in the coupled ocean–climate system. *Nat. Geosci.*, **7**, 487–492, doi:[10.1038/ngeo2188](https://doi.org/10.1038/ngeo2188).
- Tanaka, M., 1994: The onset and retreat dates of the austral summer monsoon over Indonesia, Australia and New Guinea. *J. Meteor. Soc. Japan*, **72**, 255–267.
- Torrence, C., and G. P. Compo, 1998: A practical guide to wavelet analysis. *Bull. Amer. Meteor. Soc.*, **79**, 61–78, doi:[10.1175/1520-0477\(1998\)079<0061:APGTWA>2.0.CO;2](https://doi.org/10.1175/1520-0477(1998)079<0061:APGTWA>2.0.CO;2).
- Vialard, J., G. Foltz, M. McPhaden, J.-P. Duvel, and C. de Boyer Montégut, 2008: Strong Indian Ocean sea surface temperature signals associated with the Madden-Julian oscillation in late 2007 and early 2008. *Geophys. Res. Lett.*, **35**, L19608, doi:[10.1029/2008GL035238](https://doi.org/10.1029/2008GL035238).
- , K. Drushka, H. Bellenger, M. Lengaigne, S. Pous, and J.-P. Duvel, 2013: Understanding Madden-Julian-induced sea surface temperature variations in the north western Australian basin. *Climate Dyn.*, **41**, 3203–3218, doi:[10.1007/s00382-012-1541-7](https://doi.org/10.1007/s00382-012-1541-7).
- Waliser, D. E., C. Jones, J.-K. E. Schemm, and N. E. Graham, 1999: A statistical extended-range tropical forecast model based on the slow evolution of the Madden–Julian oscillation. *J. Climate*, **12**, 1918–1939, doi:[10.1175/1520-0442\(1999\)012<1918:ASERTF>2.0.CO;2](https://doi.org/10.1175/1520-0442(1999)012<1918:ASERTF>2.0.CO;2).
- Wang, W., and M. J. McPhaden, 1999: The surface-layer heat balance in the equatorial Pacific Ocean. Part I: Mean seasonal cycle. *J. Phys. Oceanogr.*, **29**, 1812–1831, doi:[10.1175/1520-0485\(1999\)029<1812:TSLHBI>2.0.CO;2](https://doi.org/10.1175/1520-0485(1999)029<1812:TSLHBI>2.0.CO;2).
- Wentz, F. J., C. Gentemann, D. Smith, and D. Chelton, 2000: Satellite measurements of sea surface temperature through clouds. *Science*, **288**, 847–850, doi:[10.1126/science.288.5467.847](https://doi.org/10.1126/science.288.5467.847).
- Wheeler, M. C., and H. H. Hendon, 2004: An all-season real-time multivariate MJO index: Development of an index for monitoring and prediction. *Mon. Wea. Rev.*, **132**, 1917–1932, doi:[10.1175/1520-0493\(2004\)132<1917:AARMMI>2.0.CO;2](https://doi.org/10.1175/1520-0493(2004)132<1917:AARMMI>2.0.CO;2).
- Wijffels, S., and G. Meyers, 2004: An intersection of oceanic waveguides: Variability in the Indonesian Throughflow region. *J. Phys. Oceanogr.*, **34**, 1232–1253, doi:[10.1175/1520-0485\(2004\)034<1232:AIOOWV>2.0.CO;2](https://doi.org/10.1175/1520-0485(2004)034<1232:AIOOWV>2.0.CO;2).
- Zhang, C., 2005: Madden-Julian oscillation. *Rev. Geophys.*, **43**, RG2003, doi:[10.1029/2004RG000158](https://doi.org/10.1029/2004RG000158).
- , and M. Dong, 2004: Seasonality in the Madden–Julian oscillation. *J. Climate*, **17**, 3169–3180, doi:[10.1175/1520-0442\(2004\)017<3169:SITMO>2.0.CO;2](https://doi.org/10.1175/1520-0442(2004)017<3169:SITMO>2.0.CO;2).